Doping and planar defects in the formation of single-crystal ZnO nanorings

Y. Ding,[1] X. Y. Kong,[2] and Z. L. Wang[1,2,*]
[1]*School of Materials Science and Engineering, Georgia Institute of Technology, Atlanta, Georgia 30332-0245, USA*
[2]*National Center for Nanoscience and Technology, Beijing 100080, People's Republic of China*
(Received 14 February 2004; revised manuscript received 24 May 2004; published 6 December 2004)

We have recently reported the growth of freestanding, single-crystal, seamless nanorings of zinc oxide via a spontaneous self-coiling process during the growth of polar-nanobelts [X.Y. Kong *et al.*, Science **303**, 1348 (2004)]. The nanoring is made by coaxial and uniradius loop-by-loop winding of a fine ZnO nanobelt. An important fact is that each and every nanoring is made of a nanobelt that contains basal-plane planar defects, which are suggested to be important for leading the fastest growth of the nanobelt as well as lowering its elastic deformation energy. In this paper, high-resolution transmission electron microscopy is applied to investigate the nature of the planar defects in the nanobelts and in nanorings. The planar defects were initiated and formed by single-layer segregation of the doping element, such as indium, which was introduced in the growth process. The accumulation of impurity ions forms two vicinal In—O octahedral layers parallel to the basal plane. They form "head-to-head" and "tail-to-tail" polar-inversion domain boundaries. For a nanobelt that self-coils into a nanoring, we found that the head-to-head and tail-to-tail polar-inversion domain boundaries are paired, thus, the polarity of the nanobelt is unchanged. Therefore, our data support the proposed model [X.Y. Kong *et al.*, Science **303**, 1348 (2004)] that the nanoring is initiated by circularly folding a nanobelt due to long-range electrostatic interaction between the surface polar charges on the two sides, and a loop-by-loop winding of the nanobelt forms a complete ring.

DOI: 10.1103/PhysRevB.70.235408 PACS number(s): 61.46.+w, 81.07.−b

I. INTRODUCTION

The wurtzite structure family has a few important members, such as ZnO, GaN, AlN, ZnS, and CdSe, which are important materials for applications in optoelectronics, lasing, and piezoelectricity. The important characteristics of the wurtzite structure are the noncentral symmetry and the polar surfaces. The structure of ZnO, for example, can be described as a number of alternating planes composed of tetrahedrally coordinated O^{2-} and Zn^{2+} ions, stacked alternatively along the *c* axis. The oppositely charged ions produce positively charged (0001)-Zn and negatively charged $(000\bar{1})$-O polar surfaces, resulting in a normal dipole moment and spontaneous polarization along the *c* axis as well as a divergence in surface energy. To maintain a stable structure, the polar surfaces generally show facets or exhibit massive surface reconstructions, but ZnO $\pm(0001)$ is an exception, which is atomically flat, stable, and without reconstruction.[1,2] Understanding the superior stability of the ZnO $\pm(0001)$ polar surfaces is a forefront research in current surface physics.[3–6]

For a general case, one-dimensional ZnO nanostructures usually grow along the *c* axis and the side surfaces are $\{01\bar{1}0\}$ and/or $\{2\bar{1}10\}$ due to their lower energies than that of (0001),[7] resulting in the vanishment of dipole moment and much reduced piezoelectricity. The most desirable morphology to maximize the piezoelectric effect is to create nanostructures that preserve large area (0001) polar surfaces.[8,9] However, the surface energy of ZnO (0001) diverges with sample size due to the surface polarization charge. Therefore, growth of (0001) surface dominated freestanding nanostructures needs to overcome the barrier of surface energy.

To maximize the effect of polar surfaces and the piezoelectricity, nanobelts grow along $[01\bar{1}0]$ or $[2\bar{1}10]$ are preferred. We have previously reported freestanding ZnO nanobelts that grow along $[01\bar{1}0]$,[7,10] and we pointed out that the $[0\bar{1}10]$ nanobelts are always accompanied with basal plane stacking faults.[7,11] This study indicates that energy barrier set by the polar surfaces may be overcome by introducing basal-plane planar defects. In the literature, there are some reports on indium doping in ZnO ceramics.[12–15] Part of the doped In ions are accumulated in the *c* planes of ZnO to form planar defects.

Recently, we have demonstrated a large yield and high purity growth of polar surface dominated ZnO nanobelts by introducing In and/or Li ions in the raw material in the vapor–solid growth process.[16] Freestanding, single-crystal, complete nanorings of zinc oxide are formed via a spontaneous self-coiling process during the growth of polar nanobelts.[17] The nanoring is suggested to be initiated by circularly folding a nanobelt due to long-range electrostatic interaction; coaxial and uniradius loop-by-loop densely winding of the nanobelt forms a complete ring; and short-range chemical bonding among the loops results in a single-crystal structure. The self-coiling is likely to be driven by minimizing the energy contributed by polar charges, surface area, and elastic deformation. An important fact is that each and every nanoring is made of a nanobelt that has basal-plane planar defects, which are suggested to be important for leading the fastest growth of the nanobelt as well as lowing its elastic deformation energy.

In this paper, high-resolution transmission electron microscopy (HRTEM) is applied to investigate the nature of the planar defects in the nanobelts and in nanorings. The data show that the planar defects were initiated and formed by single-layer segregation of the doping element, such as indium, which was introduced in the growth process. The ac-

cumulation of impurity ions forms two vicinal In—O octahedral layers. They serve as "head-to-head" and "tail-to-tail" polar-inversion domain boundaries (IDBs). The defects are considered to take a key role in controlling the growth direction of the polar nanobelt. The head-to-head and tail-to-tail paired IDBs do not change the polarity of the nanobelt. Therefore, the nanoring is initiated by circularly folding a nanobelt due to long-range electrostatic interaction between the surface polar charges on the two sides, and a loop-by-loop winding of the nanobelt forms a complete ring. This analysis supports the mechanism proposed for the formation of nanorings.[17]

II. EXPERIMENT

Our synthesis is based on thermal evaporation of oxide powder under controlled conditions. The raw materials (ZnO powders mixed with indium oxide and lithium carbonate powders) were positioned at the highest temperature zone of a horizontal tube furnace. The source materials were then heated to 1400 °C. After a few minutes of evaporation and decomposition, the Ar carrier gas was introduced at a flux of 50 standard cubic centimeters per minute (sccm). The synthesis process was conducted at 1400 °C for 30 min. The condensation products were deposited onto a silicon substrate placed in a temperature zone of 200–400 °C under Ar pressure of 500 Torr. The single-crystal nanorings of ZnO were grown at a high reproducibility. More detailed process can be found elsewhere.[17]

The as-synthesized samples were first characterized using scanning electron microscopy (SEM) (LEO 1530 FEG at 5 kV). Gently touching a carbon film supported by a copper grid onto the silicon substrate, then the freestanding nanostructures were transferred onto the substrate surface that is ready to be studied by transmission electron microscopy (TEM). The TEM and HRTEM works were carried out using a Hitachi-2000 at 200 keV equipped with energy dispersive x-ray spectroscopy (EDS) and JEOL 4000EX at 400 kV, respectively. Cerius[2] software was used for HRTEM image simulation.

III. RESULTS

Figure 1(a) is a typical SEM image of the as-synthesized sample. Besides some nanobelts, freestanding nanorings are formed at a significant percentage. These seamless nanorings are single crystal, uniformly deformed along the circumference, and complete. The diameters of the rings are between 1 and 4 μm, with wall thickness of 10–30 nm and wall heights of 0.3–1 μm. Figure 1(b) shows a low-magnification TEM image. The uniform contrast of the two nanorings indicates that they are complete and uniform. EDS recorded from a nanoring shows presence of minor indium besides majority of Zn and O (Cu and Si signals come from copper grid and the substrate). Quantitative analysis indicates the atomic ratio of In:Zn$\approx$1:15, suggesting that In are doped in the ZnO lattice. A detailed microstructure analysis of the nanorings and their growth model were presented previously.[17] Our study here is about the structure of the planar defects in the nanorings.

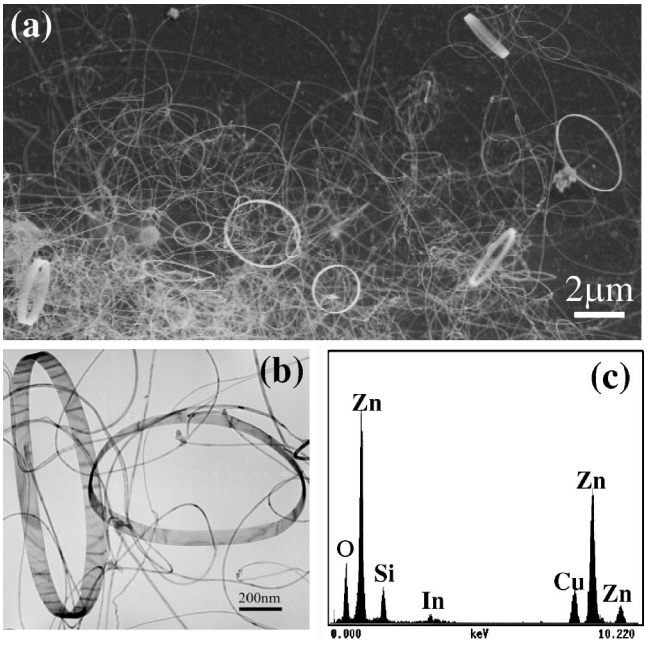

FIG. 1. (a) SEM image recorded from an as-synthesized sample, showing the presence of ZnO nanobelts and nanorings; (b) TEM image of nanorings. The typical diameter of the nanorings are 1–4 μm, thickness ~15 nm, and height 0.3–1 μm; (c) EDS spectrum recorded from a nanoring in (b), showing the presence of Zn, O, and In in the nanoring.

A. Planar defects in nanobelts

Dark-field TEM images given in Fig. 2 show three typical nanobelts. The synthesized nanobelts have a width below 30 nm. Based on the selected area electron diffraction

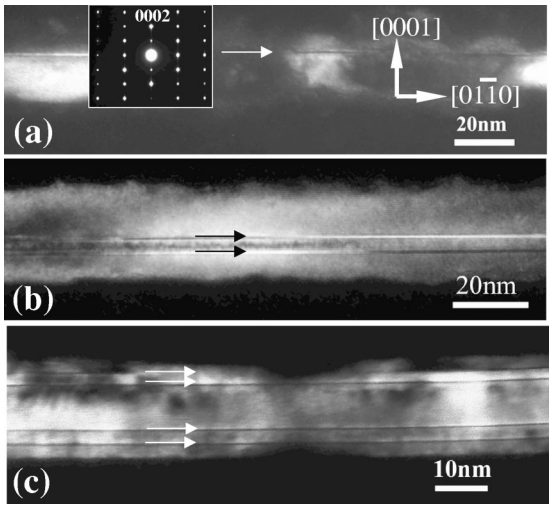

FIG. 2. Dark-field TEM images of three [01$\bar{1}$0] growth nanobelts, the inset in (a) is a selected area electron diffraction pattern recorded from the nanobelt in (a). The arrowheads point to the planar defects in each of the nanobelts.

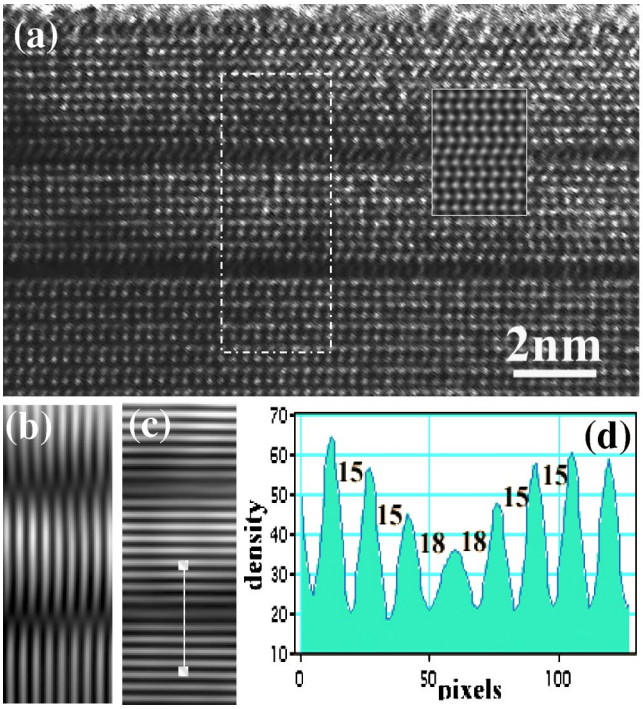

FIG. 3. (Color online) (a) HRTEM image recorded from the nanobelt shown in Fig. 2(c). The inset is a simulated image using the I_1 stacking fault model for wurtzite ZnO; (b) and (c) are Fourier filtered images of (a) using spatial frequency as $(01\bar{1}0)$ and (0002), respectively; (d) an intensity line scan across the planar defect in (c). The number is the pixels between the centers of the two adjacent peaks.

(SAED) pattern inserted in Fig. 2(a), the nanobelts grow along $[01\bar{1}0]$, with top/bottom surfaces $\pm(2\bar{1}10)$ and side surfaces $\pm(0001)$. An important fact is that the $[01\bar{1}0]$ growth nanobelts are all accompanied by planar defects. There are one, two, and four sharp-contrast planar defects along the $[01\bar{1}0]$ growth direction and in parallel to the (0001) plane, as presented by arrowheads in Figs. 2(a), 2(b), and 2(c), respectively. It indicates that the existence of planar defects is essential for forming the $[01\bar{1}0]$ growth ZnO nanobelts.

Planar defects can be twins, conventional stacking faults or interstitial stacking layer introduced by impurity atoms. Electron diffraction pattern rules out the possibility of twins. In order to determine the structure nature of the planar defects in the nanobelts, HRTEM images have been recorded from the nanobelts [see Fig. 3(a)]. Stoichiometric wurtzite structure has three types of stacking fault without any impurity, I_1, I_2, and E, which have been studied in detail.[18,19] Our simulation is based on the I_1 stacking fault for a sample thickness of 3.899 nm and objective lens defocus of −28.67 nm (Scherzer defocus for the JEOL 4000EX HR-TEM). Despite a good matching between the experimental and simulated images at the perfect lattices on the two sides, the local contrast at the planar defect in the experimental image is different from the simulated image of I_1 stacking fault. Figures 3(b) and 3(c) are the Fourier filtered images from the dashed rectangle enclosed area in Fig. 3(a) using spatial frequencies corresponding to the $(01\bar{1}0)$ and (0002) planes, respectively. Similar to the I_1 stacking fault, the $(01\bar{1}0)$ fringes have a $1/3[01\bar{1}0]$ translation across the planar defect. However, the translation in the (0002) fringes is not $\frac{1}{2}[0001]$, but slightly larger. Figure 3(d) is an intensity line scans across the planar defect, showing a 20% expansion in the planar spacing at the very adjacent of the defect. This means that the planar defect is not the stacking fault as described in the literature.[18,19] A detailed analysis on the structure of this type planar defect will be elaborated in Sec. III C.

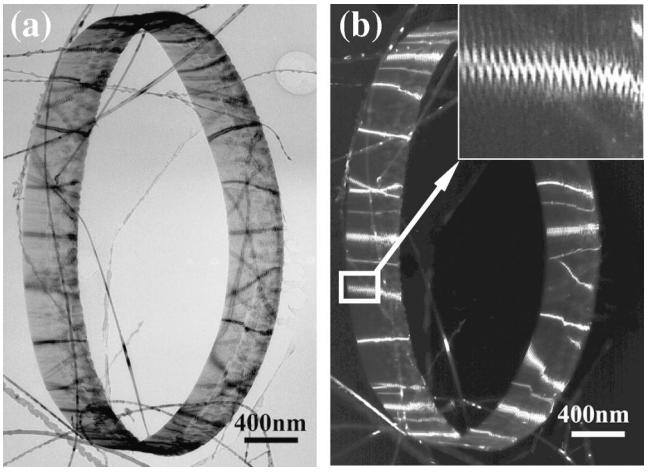

FIG. 4. (a) Bright-field and (b) dark-field TEM images recorded from a perfect nanoring. The inset in (b) is an enlarged image from the area indicated by a rectangle in (b); the contrast corresponds to the loops the nanobelt has winded to form the nanoring.

B. Planar defects in the nanorings

Planar defects are essential for the formation of nanorings. Figures 4(a) and 4(b) are bright- and dark-field TEM images of a complete nanoring. The inset in Fig. 4(b) shows the regularly spaced, sharp-contrast planar defects across the entire height of the nanoring. The periodic spacing between the defects in the nanoring represents the width of the nanobelt building block. Details about the formation of the nanoring via self-coiling of a nanobelt has been presented previously.[17]

In order to investigate the detailed structure of the defect in the nanoring, we crashed nanorings into small pieces in order to record clear HRTEM lattice images. Figure 5(a) is one of such TEM images, which shows the epitaxial and ionic bonding among the loops of the nanobelt. The SAED pattern is inserted, which shows that the radial direction of the nanoring is $[2\bar{1}10]$ (e.g., the direction pointing to the center of the ring), tangential direction of the nanoring is $[01\bar{1}0]$, and [0001] is parallel to central symmetric nanoring axis. There are two periodic spacings between the sharp-contrast planar defects, one is ~2.7 nm, and the other is ~19.0 nm [Fig. 5(b)]. The width of the nanobelt building block should be ~22 nm, and the nanobelt has two sharp-contrast planar defects, similar to the case shown in Fig. 2(b). The (0001) interface between adjacent nanobelt loops is smooth. A comparison between the two HRTEM images in

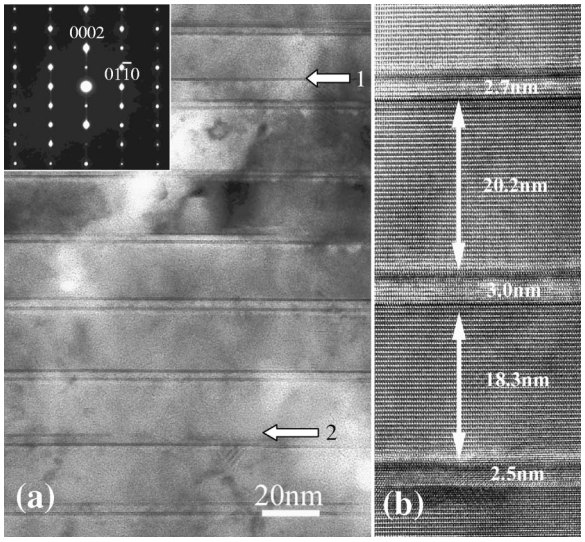

FIG. 5. (a) Low-magnification TEM image recorded from a broken nanoring; the inset is its SAED pattern; (b) HRTEM image from the nanoring, showing paired sharp-contrast planar defects.

Figs. 5(b) and 3(a) reveals that the planar defects in the two cases belong to the same type.

The image in Fig. 6(a) is recorded from a piece of another broken nanoring. The inserted SAED pattern reveals the geometric structure of the ring is the same as that presented in Fig. 5. But different from the nanoring in Fig. 5, there is only a periodic spacing among the sharp-contrast planar defects. The unit block has a width of ~18.5 nm, and the nanobelt only has a sharp-contrast planar defect as the one depicted in Fig. 2(a).

C. Structures of the planar defects: Inversion domain boundaries

Our combined EDS results and the reports on the defect microstructure in indium doped ZnO ceramics,[11–15] the planar defects in our nanobelts and nanorings may be related to

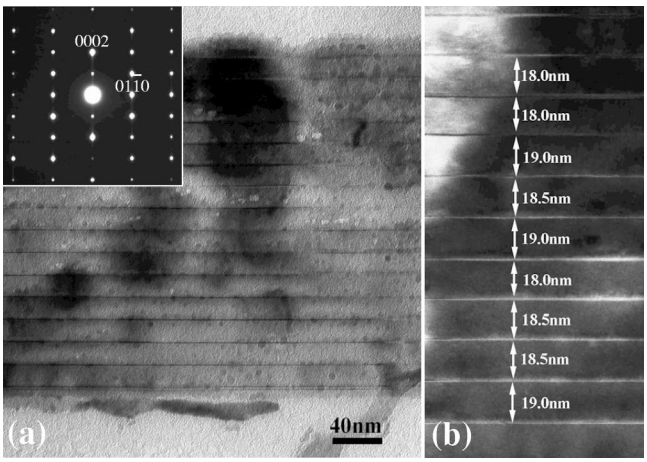

FIG. 6. (a) Low-magnification TEM image recorded from a broken nanoring; the inset is its SAED pattern; (b) higher magnification TEM image showing more detail structure.

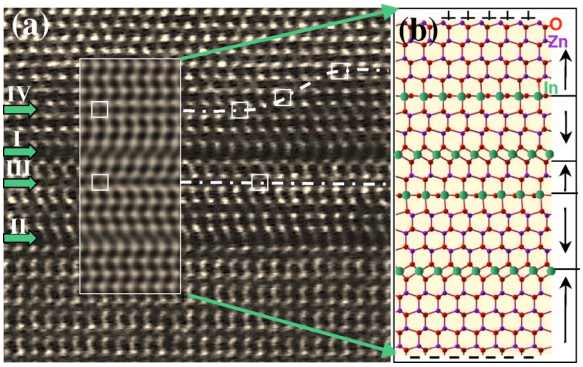

FIG. 7. (Color online) (a) HRTEM image recorded from a broken nanoring, the inset is a simulated image based on the model depicted in (b). The four green arrowheads point to four In ion layers. Four inversion domain boundaries, labeled I, II, III, and IV, have been identified in the image.

a local segregation of In ions. We now construct a model and carry out some detailed image simulations in reference to the experimental data. Figure 7(a) presents a nanobelt that has two planar defects in sharp contrast, which was recorded from a broken nanoring. If we consider the two dark layers (labeled **I** and **II** in the image) as two In—O octahedral layers, which was originally proposed by Yan *et al.*,[12] and Li et al,[15,20] we can build a model that is displayed in Fig. 7(b). If we define the (0001) surface is Zn terminated and the $(000\bar{1})$ surface is oxygen terminated, so that the polarization is along *c* axis, the two slabs on both sides of the In—O octahedral layer must have opposite polarization, which means that the In—O layer effectively induces a "head-to-head" polarization domain, so called inversion domain boundary (IDB). To configure the two sharply contrasted planar defects (**I** and **II**), there must exist another type of defect (labeled as **III**) between the **I** and **II** layers, and it should correspond to a "tail-to-tail" IDB. The **III** layer does exit in the image, and the bright spots at its very adjacent forms a rectangle pattern, as indicated by a rectangle between the **I** and **II** layers. On the other hand, based on the structural model of In_2O_3, the two slabs of ZnO on either sides of In—O octahedral layer can take not only head-to-head polarity, but also tail-to-tail polarity as presented in Fig. 7(b). In the first case, the fourfold symmetry axis of the In—O octahedra nearly lies in the ZnO *c* plane to form a head-to-head IDB. In the second case, the fourfold symmetry axis of the In—O octahedron is parallel to the ***c*** axis to form a tail-to-tail IDB. Such tail-to-tail layer also exists above the **I** layer, as labeled as **IV** layer in the image. This **IV** layer, however, does not remain in a single *c* plane, but moves across *c* planes, as indicated by a dashed line. The transverse translation of the **IV** layer may be resulted from the relocation of the doped indium ions. It is worth to notice that the translation in the [0001] direction across the tail-to-tail IDB is very small, and there is no translation along the $[01\bar{1}0]$ direction. This may be why the filtered images using spatial frequencies of $(01\bar{1}0)$ and (0002) planes show no evidence about their existence. In order to confirm our model, image simulation was carried out using dynamic electron diffraction

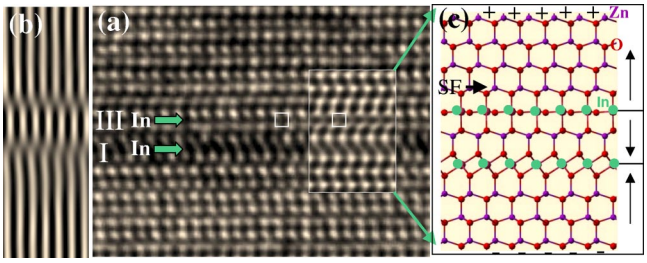

FIG. 8. (Color online) (a) HRTEM image recorded from a broken nanoring, the inset is a simulated image based on the model depicted in (c). (b) Fourier filtered image of (a) using spatial frequency of $(01\bar{1}0)$. Two inversion domain boundaries and a stacking fault have been identified in the image.

theory.[21] A simulated image based on the model in Fig. 7(b) is inserted in Fig. 7(a). The sample thickness is 2.924 nm and defocus is −28.67 nm. An excellent match between the simulated image and the experimental image supports our model.

A key fact presented by Fig. 7 is that, the top and bottom ±(0001) surfaces of the nanobelt still preserve the negative and positive ionic charges, respectively [see Fig. 7(b)], although with presence of the two inversion domain boundaries. Therefore, the polarity of the nanobelt building block is preserved! An important fact that we should point out is that the head-to-head [**I** and **II** in Fig. 7(a)] IDBs show strong contrast in the image and they are easiest to be identified; while the tail-to-tail [**III** and **IV** in Fig. 7(a)] IDBs shows rather weak contrast and they cannot be easily identified if the quality of the image is less perfect. One must be caution in identifying their existence from HRTEM images!

D. Inversion domain boundary and stacking fault

The tail-to-tail IDB sometimes can also combine with an I_1 stacking fault, to release local strain. This case is shown in Fig. 8(a). The Fourier filtered image in Fig. 8(b), which was received using the $(01\bar{1}0)$ spatial frequency, indicates that the image has another planar-defect with $1/3[01\bar{1}0]$ translation across the boundary, besides the sharp-contrast head-to-head IDB. Its contrast has a small difference from the simulated I_1 stacking fault as inserted in Fig. 3(a). Considering the four spots indicated by a rectangle for the tail-to-tail IDB [labeled **I** in Fig. 8(a)], a structure model is built in Fig. 8(c). Above the tail-to-tail IDB (**III**), the model contains an I_1 stacking fault, as indicated in Fig. 8(c). The inset in Fig. 8(a) is a simulated image using the model in Fig. 8(c), which fits the experimental image very well.

IV. DISCUSSION

A. Across-plane translation of planar defects

We now know that the sharp-contrast planar defects are head-to-head IDBs, and the weak contrasted planar defects are tail-to-tail IDBs. A tail-to-tail IDB is needed between the two adjacent head-to-head IDBs to accommodate the change in domain structure. We now look back into Fig. 5, the spacing between the two head-to-head IDBs in the nanobelt building block varies slightly, and sometime there is an extra planar defect appearing in the image (see the arrowhead 1). These phenomena may be related to the fluctuation in indium density in the local region during the growth. In the vapor-solid growth, the indium ions were sublimated from the source materials and their incoming flux may not be constant. If the indium density increases, extra head-to-head IDB may be formed [see arrowhead 1 in Fig. 5(a)]. If the indium density is decreased in the local region during the growth, the indium induced planar defect may disappear [see arrowhead 2 in Fig. 5(a)]. If there is a fluctuation in indium ion density and their distribution at the growth tip of the nanobelt, the planar defect may have a transverse translation, possibly resulting in the variation in the spacing between the planar defects, as observed in Fig. 5.

B. Formation of polar surface dominated nanobelts

If there are no planar defects, normally, the fastest growth direction of ZnO nanobelts or nanowires is [0001], forming nanobelts or nanowires without transverse polarization. Our experiments indicate that planar defects as IDBs have been introduced into ZnO nanobelts by indium ions doping. The head-to-head IDBs normally lie in the *c* plane, the exposed defect pits in $(01\bar{1}0)$ or $(2\bar{1}\bar{1}0)$ planes could be the sites that the incoming atoms tend to stick on, possibly resulting in the fastest growth along $[01\bar{1}0]$ or $[2\bar{1}\bar{1}0]$[22] and the formation of (0001) plane dominated ZnO nanobelts. Our data consistently show that the presence of planar defects is the key for the growth of polar nanobelts, and doping, e.g., In ions, is a key factor for inducing planar defects.

C. Forming or not forming a nanoring?

Our HRTEM analysis shows that the planar defects in nanorings (see Fig. 7) are always paired head-to-head and tail-to-tail IDBs. The paired IDBs do not affect the polarity of the nanobelt building block. Therefore, the nanobelt still keep opposite polar charges on its top and bottom surfaces. If the surface charges are instantaneously uncompensated during the growth, the nanobelts may tend to fold itself and interface the positively charged (0001)-Zn plane with the negatively charged (0001)-O plane, resulting in neutralization of the local polar charges and the reduced polar surface area. Thus, a loop-by-loop winding forms the nanoring structure.[17] The sketches in Fig. 9 gives the structural relationship between the nanobelt and the nanobelt folded nanoring. Being the building block, the nanobelt grows along $[01\bar{1}0]$ direction with top/bottom ±(0001) polar surfaces. Head-to-head and tail-to-tail paired IDBs formed in (0001) basal planes reserve the opposite charge statutes on the top and bottom surfaces. The formation of a nanoring can be considered as folding the nanobelt loop by loop as sketched in Fig. 9(b) and keeping the top polar surface of the first loop overlapped with the bottom opposite charged surface of the second loop.

Our experiments show a 20%–40% yield of the nanorings, and the remaining are nanobelts. There are four possible reasons, which can induce the failure of the formation

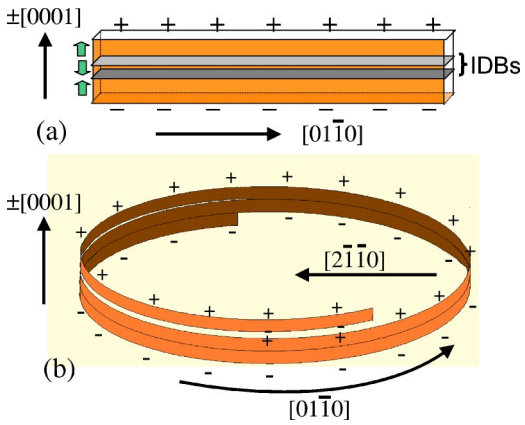

FIG. 9. (Color online) Sketch of a $[01\bar{1}0]$ growth ZnO nanobelts (a) with a head-to-head and a tail-to-tail IBDs in it; (b) sketch to show the crystallographic orientation of a nanoring.

of nanorings. First, if the head-to-head and tail-to-tail IDBs in ZnO nanobelts are not paired, which means that the top and bottom surfaces of the building block take the same kind of charges, it may not form a ring due to the repulsion among the same-charged surfaces although folding is possible. In Fig. 10, in addition to the four apparent head-to-head IDBs in the volume of the nanobelt, there are two extra head-to-head IDBs (as indicated by arrowheads) about an atomic layer next to the top and bottom side surfaces. They are so close to the surface and there is no room for forming the tail-to-tail IDBs. These two head-to-head IDBs make the exposed side surfaces of the nanobelts are all oxygen terminated (see the models in Figs. 7 and 8), resulting in the negatively charged top and bottom surfaces, thus, no nanoring will be formed. The exposed oxygen layers on both the top and bottom surfaces indicate that the flat oxygen terminated surface may be comparably stable. It is consistent with the results in Ref. 22, which show the Zn-terminated (0001) surface is chemically active while the oxygen-terminated $(000\bar{1})$ surface is inert. Second, the formation of the nanoring relies on an initiation of circular folding of the nanobelt to neutralize the interface charge, but this process is a fluctuation process during the growth. Even we have the polar surface necessary for the formation, but the fluctuation may not be there to initiate the first ring. Third, the surface charges may be compensated by the doped ions at the surfaces, thus, losing the polarization. Finally, if the nanobelt is too thick, the increased elastic deformation energy will prevent the folding of the nanobelt. In this case, no ring is formed even there is a polarization across the nanobelt. Our experimental results reveal that the ZnO nanobelts is narrow and uniform and the widths of most of them are below 30 nm. Figure 11 is a statistical plot on the widths of the nanobelt building blocks, which have been folded to form nanorings. The average width of the ZnO nanobelt building blocks is around 18.3 nm. The narrower ZnO nanobelts are highly flexibility and create much less elastic energy after the folding.

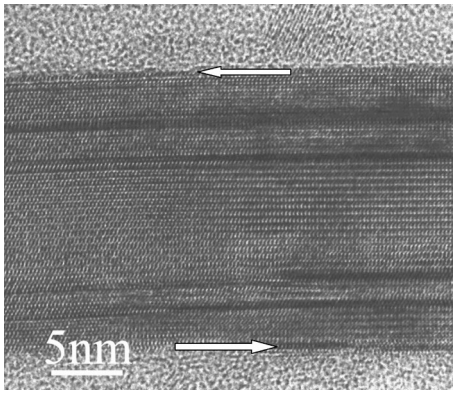

FIG. 10. HRTEM image of a nanobelt. Besides four IDBs in the nanobelt, two head-to-head IDBs are found at the very adjacent of the surface, as indicated by arrowheads.

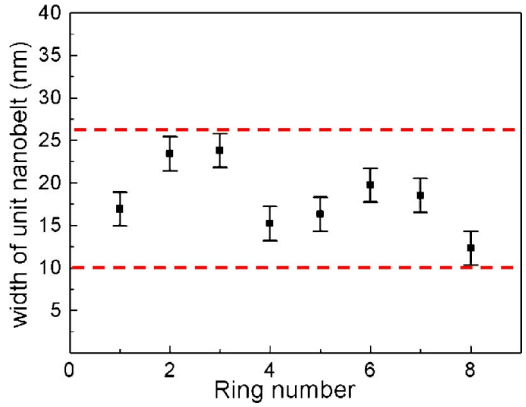

FIG. 11. (Color online) Statistical distribution on the width along [0001] of the nanobelts that have self-coiled to form nanorings.

D. Forming nanoring or nanohelical?

The folding direction of a polar nanobelt may depend on its aspect ratio. For a $[01\bar{1}0]$ growth ZnO nanobelt with side surfaces of $\pm(2\bar{1}\bar{1}0)$ and $\pm(0001)$, its folding direction is likely $[2\bar{1}\bar{1}0]$ due to its wider dimension across the $(2\bar{1}\bar{1}0)$ plane than that across the (0001) plane. This type of configuration is favorable of forming complete nanorings.[17] If the folding direction is [0001], no complete nanoring would be formed, but possibly helical nanosprings.[16]

For a $[2\bar{1}\bar{1}0]$ growth ZnO nanobelt with side surfaces of $(01\bar{1}0)$ and $\pm(0001)$, if its folding direction is $[01\bar{1}0]$, a nanoring may be formed. If its folding direction is [0001], a nanohelical/nanospring may be formed. For this type of nanobelt, we have only observed the formation of nanohelicals.[16]

From the energy point of view, we anticipate that a formation of planar defects may reduce the bending modulus of the nanobelt, so that much less elastic energy is created when bending into an arc. Theoretical calculations are required to prove this assumption.

As we pointed out in the experimental session, lithium was also introduced. It was reported that Li can improve the resistivity of ZnO film and is likely to be present in the volume as point substitution of Zn.[23,24] Due to the difficulty

in detecting low-concentration lithium by the available analytical techniques, we are not sure if Li has been doped into the nanobelts. More work is needed to define its role in nanoring formation.

V. CONCLUSION

As a continuation of our report on the formation of ZnO nanorings,[17] this paper is devoted to systematically investigate the planar defect structures in ZnO nanobelts and ZnO nanorings. We found that the planar defects are mostly due to the segregation of doping element. With the accumulation of doped indium ions in ZnO *c* planes, head-to-head and tail-to-tail inversion domain boundaries (IDBs) can be formed. The head-to-head IDBs have sharp contrast and always keep in a single **c**-plane, while the tail-to-tail IDBs have very weak contrast and can easily creep across the *c* planes. These IDBs are considered to take a key role in controlling the growth direction of the ZnO nanobelts. Although the polarity will be inverted across a single IDB, head-to-head and tail-to-tail paired IDBs in the building blocks of nanorings do not change its polarity, making it possible to form nanorings to neutralize the interfacial charge. This study supports our nanoring formation model.[17]

ACKNOWLEDGMENTS

Thanks to the financial support of the NASA Vehicle Systems Program and Department of Defense Research and Engineering (DDR&E), and the Defense Advanced Research Projects Agency for support of this research. This material is based upon work supported by the Space and Naval Warfare Systems Center San Diego under Award No. N66001-04-1-8903.

*Author to whom correspondence should be addressed; electronic address: zhong.wang@mse.gatech.edu

[1] O. Dulub, L. A. Boatner, and U. Diebold, Surf. Sci. **519**, 201 (2002).
[2] B. Meyer and D. Marx, Phys. Rev. B **67**, 035403 (2003).
[3] P. W. Tasker, J. Phys. C **12**, 4977 (1979).
[4] O. Dulub, U. Diebold, and G. Kresse, Phys. Rev. Lett. **90**, 016102 (2003).
[5] A. Wander, F. Schedin, P. Steadman, A. Norris, R. McGrath, T. S. Turner, G. Thornton, and N. M. Harrison, Phys. Rev. Lett. **86**, 3811 (2001).
[6] V. Staemmler, K. Fink, B. Meyer, D. Marx, M. Kunat, S. Gil Girol, U. Burghaus, and Ch. Woll, Phys. Rev. Lett. **90**, 106102 (2003).
[7] Z. W. Pan, Z. R. Dai, and Z. L. Wang, Science **291**, 1947 (2001).
[8] A. D. Corso, M. Posternak, R. Resta, and A. Baldereschi, Phys. Rev. B **50**, 10 715 (1994).
[9] F. Bernardini, V. Fiorentini, and D. Vanderbilt, Phys. Rev. B **56**, R10 024 (1997).
[10] P. Gao, Y. Ding, and Z. L. Wang, Nano Lett. **3**, 1315 (2003).
[11] Z. L. Wang, Z. W. Pan, and Z. R. Dai, Microsc. Microanal. **8**, 467 (2002).
[12] Y. Yan, S. J. Pennycook, J. Dai, R. P. H. Chang, A. Wang, and T. J. Marks, Appl. Phys. Lett. **73**, 2585 (1998).
[13] M. A. McCoy, R. W. Grimes, and W. E. Lee, Philos. Mag. A **76**, 1187 (1997).
[14] P. J. Cannard and R. J. D. Tilley, J. Solid State Chem. **73**, 418 (1988).
[15] C. Li, Y. Bando, M. Nakamura, and N. Kimizuka, Micron **31**, 543 (2000).
[16] X. Y. Kong and Z. L. Wang, Nano Lett. **3**, 1625 (2003).
[17] X. Y. Kong, Y. Ding, R. S. Yang, and Z. L. Wang, Science **303**, 1348 (2004).
[18] V. Potin, P. Ruterana, and G. Nouet, J. Phys.: Condens. Matter **12**, 10301 (2000).
[19] C. Stampfl and C. G. Van de Walle, Phys. Rev. B **57**, R15 052 (1998).
[20] C. Li, Y. Bando, M. Nakamura, and N. Kimizuka, J. Electron Microsc. **46**, 119 (1997).
[21] J. M. Cowley and A. Moodie, Acta Crystallogr. **10**, 609 (1957).
[22] W. J. Li, E. W. Shi, W. Z. Zhong, and Z. W. Yin, J. Cryst. Growth **203**, 186 (1999).
[23] E. D. Kolb and R. A. Laudise, J. Am. Ceram. Soc. **48**, 342 (1965).
[24] W. Water, S. Y. Chu, Y. D. Juang, and S. J. Wu, Mater. Lett. **57**, 998 (2002).